Runaway electrons and the evolution of the plasma current in tokamak disruptions

H. Smith
Department of Radio and Space Science, Chalmers University of Technology, SE-412 96 Göteborg, Sweden

P. Helander
EURATOM/UKAEA Fusion Association, Culham Science Centre, Abingdon OX14 3DB, United Kingdom

L.-G. Eriksson
Association EURATOM-CEA, CEA/DSM/DRFC, CEA-Cadarache, F-13108 St. Paul lez Durance, France

D. Anderson, M. Lisak, and F. Andersson
Department of Radio and Space Science, Chalmers University of Technology, SE-412 96 Göteborg, Sweden

(Received 13 July 2006; accepted 1 September 2006; published online 11 October 2006)

After the thermal quench of a tokamak disruption, the plasma current decays and is partly replaced by runaway electrons. A quantitative theory of this process is presented, where the evolution of the toroidal electric field and the plasma current is calculated self-consistently. In large tokamaks most runaways are produced by the secondary (avalanche) mechanism, but the primary (Dreicer) mechanism plays a crucial role in providing a "seed" for the avalanche. As observed experimentally, up to 50%–60% of the plasma current is converted into runaways in the Joint European Torus [P. H. Rebut *et al.*, Nucl. Fusion **25**, 1011 (1985)], and the conversion is predicted to be somewhat larger in ITER [R. Aymar *et al.*, Plasma Phys. Controlled Fusion **44**, 519 (2002)]. Furthermore, the postdisruption current profile is found to be more peaked than the predisruption current—so much, in fact, that the central current density can increase although the total current falls. It is also found that the runaway current profile easily becomes radially filamented. These results may have implications for the stability of the postdisruption plasma. © *2006 American Institute of Physics*. [DOI: 10.1063/1.2358110]

I. INTRODUCTION

One of the major problems facing the development of large tokamaks is the frequent occurrence of plasma disruptions. In addition to causing enormous mechanical and thermal loads on the vessel, disruptions often lead to the acceleration of "runaway" electrons, which can damage the first wall on impact. This is potentially a more serious problem in ITER (Ref. 1) than in present experiments since the efficiency of the dominant runaway production mechanism (discussed below) increases exponentially with plasma current.

Following the thermal quench of the disruption, the predisruption current carried by thermal electrons decays and is partly replaced by a current of runaway electrons. This phenomenon has been observed in many tokamaks over the years, and in the largest present-day devices, the Joint European Torus (JET) (Ref. 2) and JT-60U (Ref. 3), up to about half the plasma current is converted to runaways in this way. However, until recently there has been little quantitative understanding of this process. Runaway electron theory has traditionally focused on the physical mechanisms for fast electron generation and how efficient these mechanisms are, but relatively little effort has been devoted to analyzing the consequences for the evolution of the current and the interplay between the runaway population and the electric field in a tokamak disruption. This is the topic of the present paper, where we endeavor to calculate the postdisruption runaway current profile from predisruption plasma parameters. In doing so, it is crucial to treat the toroidal electric field in a consistent manner. This field is initially induced by the dramatic increase in the plasma resistivity that takes place due to the drop in electron temperature during the thermal quench. The electric field accelerates runaways, whose rising current limits the further growth of the field. Since the runaways thus modify the electric field responsible for their own creation, the system is nonlinear and exhibits mathematically interesting behavior. The complexity of this behavior is further enhanced by the fact that the growth rate of the runaway population is comparable to the resistive diffusion rate of the electric field. This field thus diffuses through the plasma whilst generating the runaway current and being modified thereby at the same time.

In Sec. II, we introduce the physics elements that go into the calculation of these processes, and we discuss the simplifications that are (necessarily) adopted to make the system tractable. The result is a set of two-coupled, nonlinear differential equations: one for the runaways and one for the electric field. In the Appendix, a yet simpler, "zero-dimensional" version of these equations is used to derive a criterion, involving only predisruption plasma parameters and the postdisruption electron temperature, that indicates whether or not a substantial part of the plasma current can be expected to be converted into a runaway current. In Sec. III, we solve the more complete model equations derived in Sec. II numerically for a number of experimentally relevant situations. A number of interesting results emerge from these calculations. First, the time scale and efficiency of runaway generation

agree with those observed in experiments if the postdisruption temperature is taken to be around 10 eV. This temperature cannot be measured in the experiments, but has been conjectured to be in this range on other grounds.[4] Second, it is found that the current profile evolves in a nontrivial way as the runaways are generated. The postdisruption runaway current profile can become more peaked on the magnetic axis than the predisruption current, which could have important consequences for the stability of the postdisruption plasma. Third, it is found that the runaway current can easily become filamented in the radial direction because of the high sensitivity of runaway generation to plasma parameters. These numerical results suggest ways in which the system can be simplified and analytical understanding can be gained, which is done in Sec. IV. Here a nonlinear ordinary differential equation is derived which relates predisruption plasma parameters to the postdisruption runaway current profile. Although a general solution of this equation cannot be constructed, it is possible to extract a number of important properties from it which illuminate the numerical results of the previous section. Our conclusions are summarized in the final section, where a qualitative comparison with experience from experiments is also undertaken.

Some of our results have recently been published more briefly elsewhere.[5–7] In the present paper we present a fuller picture by showing many more numerical results and developing the analytical theory in greater detail.

II. THE MODEL

A tokamak disruption is usually initiated by a large-scale instability that causes the plasma to interact with the first wall. We do not consider this initial stage of the disruption, but focus our attention on what happens next. The plasma quickly regains axisymmetry but loses nearly all its thermal energy in the ensuing thermal quench, which typically lasts less than 1 ms. The resulting increase in resistivity causes a large toroidal electric field $E_\phi \simeq E_\parallel$ to be induced, which in some disruptions accelerates runaway electrons to relativistic energies. At the same time, this electric field diffuses through the resistive plasma and continues to generate new runaways until it drops below the cutoff field E_c below which no runaway generation can occur.[8] Towards the end of the disruption virtually all current is carried by runaways, since the remaining electric field is too weak to drive any significant Ohmic current in the cold resistive plasma.

The evolution of the current is thus governed by two distinct processes: runaway electron generation and electric-field diffusion. The former of these occurs, in turn, by two different mechanisms, which we shall refer to as primary and secondary runaway generation, respectively. Primary (or "Dreicer") generation[9] is caused by a Fokker-Planck diffusion process in velocity space producing runaways at the rate[8,10]

$$\dot{n}_r^{\mathrm{I}} \simeq \frac{n_e}{\tau}\left(\frac{m_e c^2}{2T_e}\right)^{3/2}\left(\frac{E_{\mathrm{D}}}{E_\parallel}\right)^{3(1+Z_{\mathrm{eff}})/16} \times \exp\left(-\frac{E_{\mathrm{D}}}{4E_\parallel} - \sqrt{\frac{(1+Z_{\mathrm{eff}})E_{\mathrm{D}}}{E_\parallel}}\right), \tag{1}$$

where $\tau = 4\pi\varepsilon_0^2 m_e^2 c^3/(n_e e^4 \ln\Lambda)$ is the relativistic electron collision time[11] and $E_{\mathrm{D}} = m_e^2 c^3/(e\tau T_{\mathrm{e}})$ is the Dreicer field. Secondary (or "avalanche") runaway generation is caused by collisions at close range between existing runaway electrons and thermal ones, and produces runaways at the rate[12]

$$\dot{n}_r^{\mathrm{II}} \simeq n_r \frac{E_\parallel/E_c - 1}{\tau \ln\Lambda}\sqrt{\frac{\pi\varphi}{3(Z_{\mathrm{eff}}+5)}} \times \left(1 - \frac{E_c}{E_\parallel} + \frac{4\pi(Z_{\mathrm{eff}}+1)^2}{3\varphi(Z_{\mathrm{eff}}+5)(E_\parallel^2/E_c^2 + 4/\varphi^2 - 1)}\right)^{-1/2}, \tag{2}$$

where $E_c = m_e c/(e\tau)$, $\varphi = 1 - 1.46\epsilon^{1/2} + 1.72\epsilon$, and $\epsilon = r/R$ is the inverse aspect ratio. In the following we will assume that $Z_{\mathrm{eff}} = 1$, $\varphi \simeq 1$, and $E_\parallel \gg E_c$ and use the approximate expression

$$\dot{n}_r^{\mathrm{II}} \simeq n_r\left(\frac{\pi}{2}\right)^{1/2}\frac{E/E_c - 1}{3\tau\ln\Lambda}, \tag{3}$$

where the small term of unity in the numerator has been retained to ensure that no runaways are produced for $E_\parallel < E_c$. This "critical" electric field corresponds to the friction force on a relativistic electron, and no runaway acceleration can occur unless $E_\parallel > E_c$ (Ref. 8). Because the rate of secondary runaway production is proportional to n_r, it causes the runaway density to increase exponentially with the consumed magnetic flux, which is the origin of the term "avalanche." The role of secondary runaway generation is therefore to amplify a preexisting "seed" population of runaways.

There are other runaway generation mechanisms that could be important, especially in ITER (Ref. 13). Tritium decay can provide a source of fast electrons, as well as Compton scattering of γ rays emitted by the activated wall, and if the thermal quench is very rapid, the high-energy tail of the initial electron distribution can be converted into a burst of runaway production.[14] However, in the present paper the primary and secondary generation mechanisms are assumed to be dominant. For simplicity, radial diffusion of runaway electrons due to magnetic-field fluctuations will also be neglected. Adding the two contributions to runaway generation in Eqs. (1) and (3) gives the first model equation, describing the total runaway production

$$\dot{n}_r = \dot{n}_r^{\mathrm{I}} + \dot{n}_r^{\mathrm{II}}. \tag{4}$$

The temporal evolution of the induced electric field is governed by the parallel component of the induction equation

$$\nabla^2 \mathbf{E} = \mu_0 \frac{\partial \mathbf{j}}{\partial t}, \tag{5}$$

which gives a second model equation. For simplicity, we neglect toroidal effects and approximate the plasma column

by a circular cylinder where the field lines run approximately in the axial direction, so that

$$\frac{1}{r}\frac{\partial}{\partial r}\left(r\frac{\partial E_\parallel}{\partial r}\right)=\mu_0\frac{\partial j_\parallel}{\partial t}, \tag{6}$$

where r is the radial coordinate. The current density $j_\parallel$ consists of both the Ohmic current and the current carried by runaways electrons. A simple model for the latter is obtained by assuming that all runaways travel at the speed of light. This neglects the time required to accelerate a newly generated runaway electron to relativistic speeds, which is justified if most runaways are created by the secondary mechanism since the acceleration time $t_{\rm acc}\sim m_e c/eE_\parallel=\tau E_c/E_\parallel$ is then shorter than the avalanche growth time $t_{\rm av}\sim\tau\ln\Lambda E_c/E_\parallel$. The total current density becomes $j_\parallel=\sigma_\parallel E_\parallel+n_r ec$, where $\sigma_\parallel$ is the Spitzer conductivity $\sigma_{\rm Sp}=3\varepsilon_0^2(2\pi T_e)^{3/2}/(0.51m_e^{1/2}e^2\ln\Lambda)$ times a neoclassical correction,[15]

$$\sigma_\parallel=\sigma_{\rm Sp}\frac{(1-\phi)(1-C\phi)}{Z_{\rm eff}}\frac{1+0.47(Z_{\rm eff}-1)}{1+0.27(Z_{\rm eff}-1)}, \tag{7}$$

where

$$C=\frac{0.56}{Z_{\rm eff}}\left(\frac{3.0-Z_{\rm eff}}{3.0+Z_{\rm eff}}\right), \tag{8}$$

$$\phi=f_{\rm T}\left[1+(0.58+0.20Z_{\rm eff})\frac{2Rq\epsilon^{-3/2}}{3\sqrt{2\pi}c\tau}\left(\frac{m_e c^2}{T_e}\right)^2\right]^{-1}, \tag{9}$$

and the fraction of trapped electrons is approximately $f_{\rm T}=1-(1-\epsilon)^2/[(1-\epsilon^2)^{1/2}(1+1.46\epsilon^{1/2})]$.

It is convenient to normalize the dependent and independent variables by writing

$$n(t,r)\equiv\frac{n_r(t,r)ec}{\bar{j}_{\parallel 0}}, \tag{10}$$

$$E(t,r)\equiv\frac{E_\parallel(t,r)}{\bar{E}_{c0}}, \tag{11}$$

$$t'\equiv\frac{t}{\sqrt{2/\pi}3\bar{\tau}_0\ln\Lambda}, \tag{12}$$

where an overhead bar denotes an on-axis quantity and a subscript zero signifies a predisruption value. We also introduce the following normalized parameters:

$$u^2(t,r)\equiv\frac{\bar{E}_{c0}}{E_{\rm D}(t,r)}=\frac{T_e}{m_e c^2}\frac{\bar{n}_{e0}}{n_e}, \tag{13}$$

$$\alpha\equiv(2\pi)^{3/2}\frac{\bar{j}_{\parallel 0}a^2}{3\ln\Lambda I_{\rm A}}, \tag{14}$$

$$\sigma(t,r)\equiv\frac{\bar{E}_{c0}}{\bar{j}_{\parallel 0}}\sigma_\parallel, \tag{15}$$

where $I_{\rm A}=4\pi m_e c/(\mu_0 e)$ is the Alfvén current. The parameter α is closely related to the conventional estimate of the number of exponentiations in the avalanche, $I_0/(I_{\rm A}\ln\Lambda)$ (Ref. 12), and is large in tokamaks with large current, such as ITER. The equations [(4) and (6)] for runaway generation and induction can now be rewritten in the normalized quantities as a system of two coupled partial differential equations,

$$\frac{\partial n}{\partial t'}=\left[F(E,t,x)+n\left(E-\frac{n_e}{\bar{n}_{e0}}\right)\right]\Theta\left(E-\frac{n_e}{\bar{n}_{e0}}\right), \tag{16}$$

$$\frac{1}{\alpha x}\frac{\partial}{\partial x}x\frac{\partial E}{\partial x}=\frac{\partial}{\partial t'}(\sigma E+n), \tag{17}$$

where $x=r/a$ is normalized plasma radius and Θ is a Heaviside step function preventing runaway acceleration if $E<n_e/\bar{n}_{e0}$, i.e., if $E_\parallel<E_c$. Primary generation is in Eq. (16) represented by the function $F(E,t,x)$, which in the simple case when $Z_{\rm eff}=1$ becomes

$$F(E,t,x)\equiv\frac{3\ln\Lambda}{2\sqrt{\pi}}\frac{\bar{n}_{e0}ec}{\bar{j}_{\parallel 0}}\frac{\sqrt{n_e/\bar{n}_{e0}}}{u^{15/4}E^{3/8}}\times\exp\left(-\frac{1}{4u^2E}-\sqrt{\frac{2}{u^2E}}\right). \tag{18}$$

The boundary conditions for $n(t,x)$ and $E(t,x)$ are $n(t,1)=0$ and $E(t,1)=0$ if the plasma is surrounded by a perfectly conducting wall at $r=a$. If the wall is instead located at $r=b>a$, the boundary condition for $E(t,1)$ is obtained by matching to the vacuum solution $E(t,x)\propto\ln(ax/b)$ giving $E(t,1)+\ln(b/a)dE/dx(t,1)=0$.

The conductivity σ is specified externally in Eqs. (16) and (17). The Ohmic electric field required to drive the predisruption current is usually smaller than critical, $E_\parallel<E_c$, so that Eqs. (16) and (17) predict a steady state $\partial n/\partial t'=\partial E/\partial t'=0$ prior to the disruption. At the thermal quench, the conductivity σ suddenly drops, causing a change in the right-hand side of Eq. (17). The subsequent evolution of the system will be investigated numerically in Sec. III. Of particular interest is the new, postdisruption steady state that is reached long after the thermal quench, in practice about 10–20 ms afterwards. In this state, all remaining current is carried by runaways, and it is of interest to characterize its magnitude and radial profile.

Before we present numerical solutions of the model equations [(16) and (17)] in Sec. III, it is useful to discuss what conclusions can be drawn from the simpler, zero-dimensional model that has been used previously in the literature.[5,16–18] It was shown in Ref. 5 that such a model leads to a simple criterion for under which conditions many runaways will be produced. This theory is improved in the Appendix and the result is that substantial runaway production occurs if the parameter H, defined in Eq. (A10), is positive. This criterion is compared with numerical solutions of Eqs. (16) and (17) in the next section.

III. NUMERICAL SIMULATIONS

The full system of model equations [(16) and (17)], unlike its zero-dimensional counterpart in the Appendix, retains

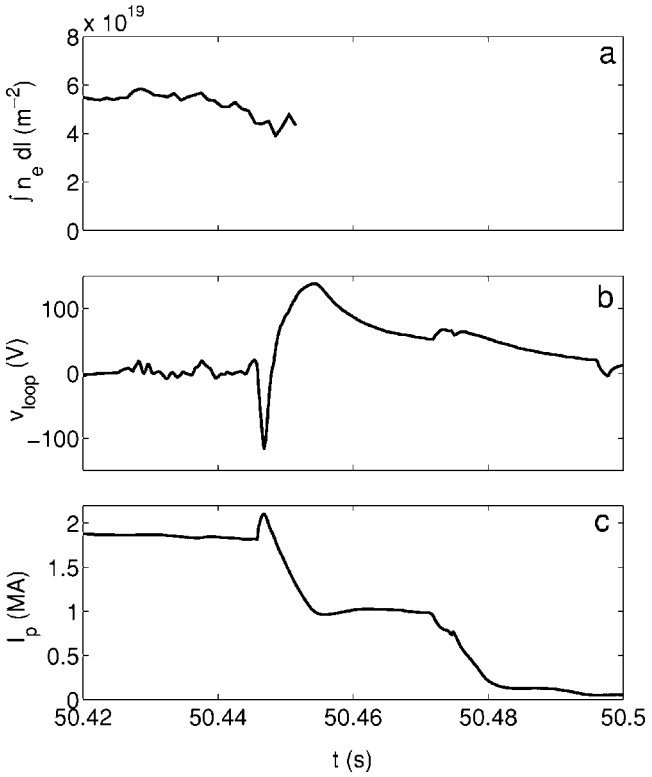

FIG. 1. Data from JET discharge 63 133 at the time of the disruption: (a) line-integrated density, (b) loop voltage at the vessel wall, (c) plasma current.

information about the radial profiles of the current and electric field. We shall adopt the following model of the temperature decay during the thermal quench:

$$T_e(t,x) = T_{\text{final}}(x) + [T_0(x) - T_{\text{final}}(x)]e^{-t/t_0}, \tag{19}$$

and solve numerically for the evolution of the runaway electron density $n(t,x)$ and the electric field $E(t,x)$. This has been done for a number of cases using explicit time stepping and finite differences to approximate the derivatives.

A. JET

We begin by presenting the results of a numerical simulation where the parameters are chosen to match a particular, but typical, JET disruption experiment discharge with deuterium (No. 63133): $I_0=1.86$ MA, $B=3$ T, $t_0=0.5$ ms, $R=3$ m, $a=1$ m, central $q\simeq 1.5$, $n_e(x,t)=(1-0.9x^2)^{2/3}\cdot 2.8\cdot 10^{19}$ m^{-3}, $T_0=(1-0.9x^2)^2\cdot 3.1$ keV, $T_{\text{final}}=(1-0.9x^2)\cdot 10$ eV. The final temperature is poorly diagnosed in the experiment, not least because of the contribution from runaways to the electron cyclotron emission. The radial profile of the final temperature is here assumed to be flatter than the initial one. Experimental data from discharge 63 133 is presented in Fig. 1. The line-integrated density measured by an interferometer is shown in Fig. 1(a) (normal accuracy ±10%); the line of sight passes close to the center of the tokamak. Owing to uncertainties (mainly due to fringe jumps) in the signal after the Ohmic current quench, it is shown only up to the end of this phase. The signal does not indicate any significant change in the density in the phase

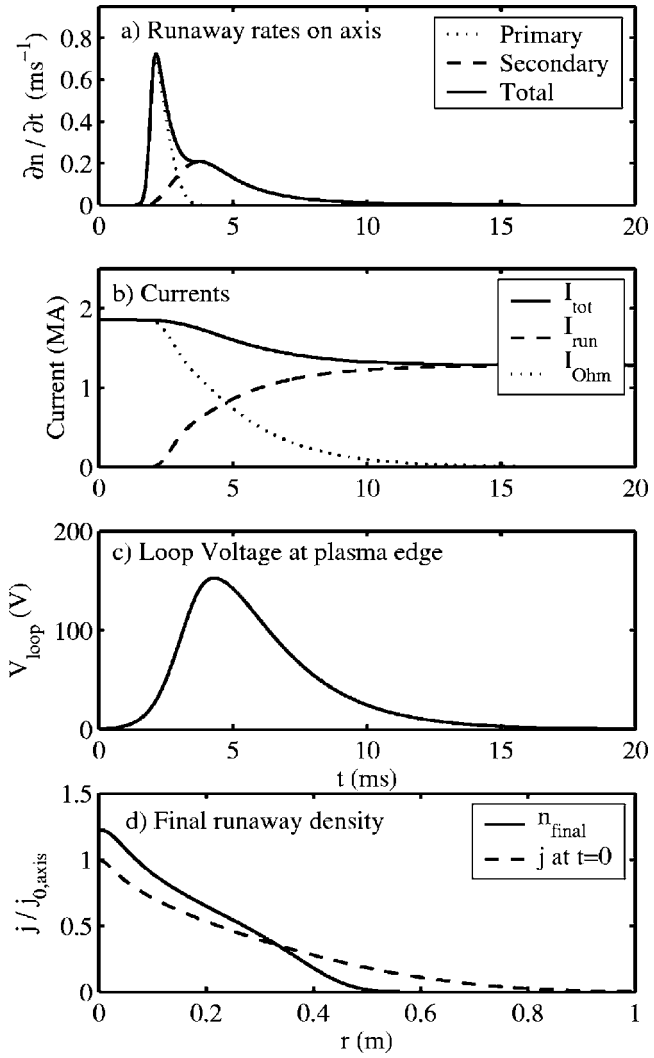

FIG. 2. A simulation of the runaway dynamics in JET discharge 63 133.

before the runaway generation. However, since it is a line-integrated measurement one cannot rule out that the density profile changed. Nevertheless, we have, for simplicity, taken the density to be constant in the present simulation. Moreover, we emphasize that we do not study the very first stage of the disruption, which is characterized by magnetohydrodynamic (MHD) instability. During this phase, the loop voltage exhibits a characteristic negative spike and the current a small transient increase, as clearly visible in Figs. 1(b) and 1(c). Tomographic reconstruction indicates that the plasma quickly regains axisymmetry,[18] after which the current decays and the runaway electron beam is formed and shows up as the current "plateau" in Fig. 1(c) that lasts from about $t=50.455$ s to $t=50.47$ s. In discharges that are more stable (JT-60U and the predivertor JET), this postdisruption runaway current can persist for a very long time, sometimes several seconds.[19]

Turning to the outcome of the simulation, Fig. 2 shows that the initial plasma current, $I_0=1.86$ MA, is converted to a runaway current of 1.3 MA in the simulation [as compared with 1.1 MA in the experiment; see Fig. 1(c)], with 3/8 of the runaways produced by the primary mechanism and the

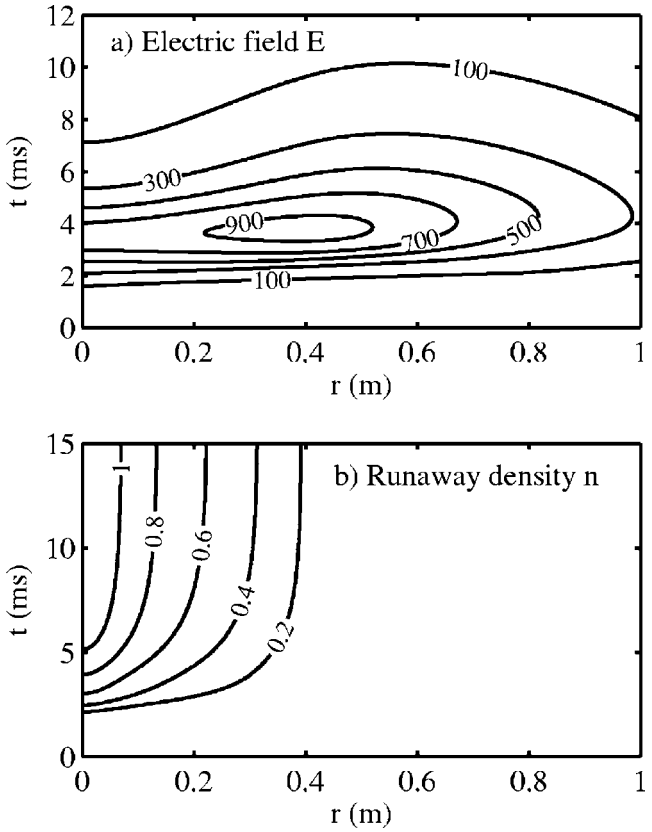

FIG. 3. Contour plots of (a) the normalized electric field and (b) the normalized runaway density from a simulation of the runaway dynamics in the disruption in JET discharge 63 133.

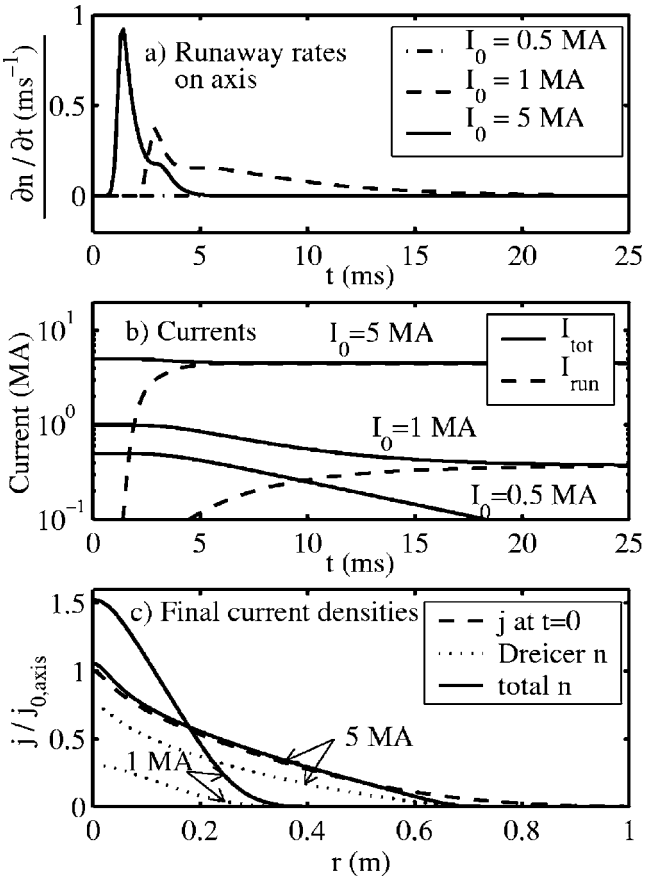

FIG. 4. For the three cases I_0=0.5 MA (H=0.1), I_0=1 MA (H=7.7), and I_0=5 MA (H=25): (a) On-axis runaway production rates. (b) Evolution of the runaway current and the total (runaway+Ohmic) current. (c) The accumulated primary runaway density profile (dotted) and the final runaway density profile in the postdisruption steady state (solid). The initial current profile (dashed) is shown for reference. Note that the runaway production in the I_0=0.5 MA case is too low to be seen on the scales of the figures.

remaining 5/8 by the avalanche. The time scale on which the current drops and the loop voltage at the plasma edge rises [Figs. 2(b) and 2(c)] are also in approximate agreement with the experiment [Figs. 1(b) and 1(c)]. Even better agreement can be obtained by tweaking the postdisruption parameters in the simulations, but there seems to be little meaning in doing this in view of the considerable experimental uncertainties of these parameters.

The simulation also shows that the postdisruption current density is more peaked in the center of the plasma than the initial thermal current [see Fig. 2(d)]. In fact, the current density actually increases on the magnetic axis although the total current falls. This phenomenon was first reported in Refs. 6 and 20, and is likely to have implications for the MHD stability of the postdisruption plasma. The reason for the current density peaking is that runaway generation is most efficient in the center of the plasma, so that the growth of the electric field is first limited there by the runaways "short circuiting" the plasma current. Some time after the thermal quench, the electric field therefore has an off-axis maximum [see Fig. 3(a)], causing inward diffusion of the field and consequently an increased runaway production near the magnetic axis.

Further physical insight can be gained by running several simulations and studying how the current and runaway dynamics are affected by varying different disruption parameters. In the following we present qualitative and quantitative results of such a parameter scan around the reference discharge just described.

First, we investigate the effects of varying the initial current I_0. Physically, this affects both the primary and secondary runaway production mechanisms. The electric field just after the thermal quench depends on I_0, since it is proportional to the initial electric field $E_{\|0}=j_{\|0}/\sigma_{\|0}$, so a low initial current causes a small primary production. The potential number of exponentiations in the avalanche increases with increasing I_0, since the parameter α is proportional to $j_{\|0}$, which implies that electric-field diffusion is slow compared to avalanche growth when I_0 is high. Figure 4 shows that when $I_0 \lesssim 0.5$ MA primary production is too small to initiate an avalanche that is able to produce any significant runaway current. At moderate values of I_0 (0.5–5 MA), there are enough primary "seed" runaways to produce a large avalanche, and hence the final current profile becomes peaked on axis [Fig. 4(c)]. For sufficiently high I_0 ($\gtrsim$5 MA), primary generation is large enough to short circuit the plasma without the need for avalanche runaways. The final runaway current profile then reproduces the initial current profile.

The same pattern can be recognized when n_{e0} or T_{final} are

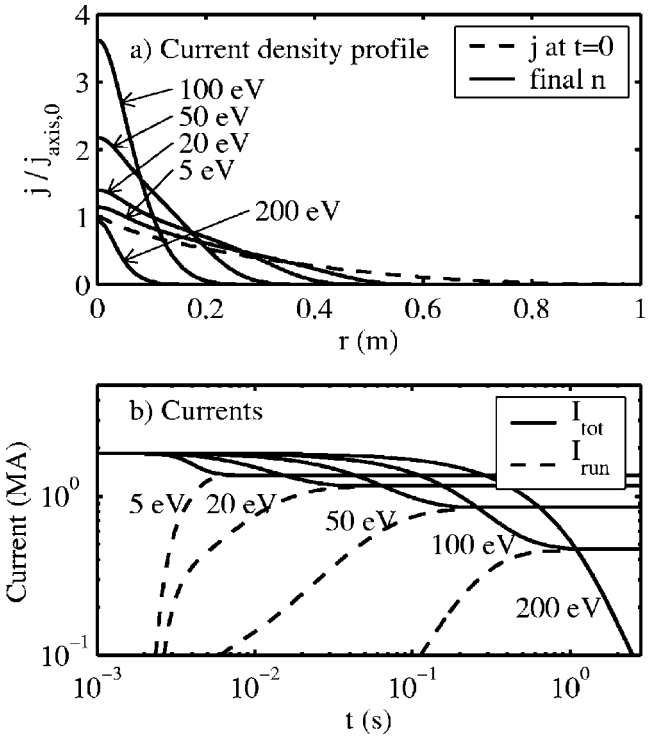

FIG. 5. For the five cases $T_{\text{final}}=5$ eV ($H=15$), 20 eV ($H=11$), 50 eV ($H=7.7$), 100 eV ($H=4.0$), and 200 eV ($H=-0.8$): (a) The final runaway current profiles and (b) the evolution of the runaway current and the total current.

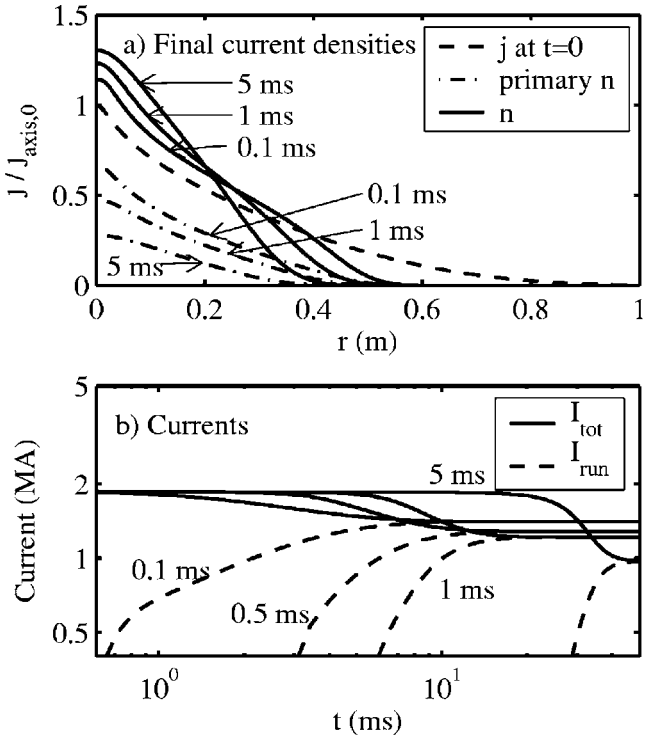

FIG. 6. (a) The primary runaway and total runaway current profiles and (b) the currents for simulations with the different thermal quench times $t_0=0.1$, 0.5, 1, and 5 ms. Long thermal quench times give lower final current.

varied. These parameters both affect the primary generation through the factor $E_{\|}/E_{\text{D}}$. One generally finds that the parameter space can be divided into three main regions: one with very low runaway production ($n_{e0}\gtrsim 10^{20}$ m^{-3}, $T_{\text{final}}\gtrsim 200$ eV, $I_0\lesssim 0.5$ MA), a second, middle region with high on-axis runaway current peaking and predominantly secondary generation, and a third where primary generation is effective enough to reproduce the initial current profile ($n_{e0}\lesssim 10^{19}$ m^{-3}, $T_{\text{final}}\lesssim 10$ eV, $I_0\gtrsim 5$ MA). The transition between the first and second regions is found to appear approximately where the parameter H is zero. However, it is not a very sharp transition, especially when I_0 is varied, because the underlying assumption that the thermal quench time is much shorter than the diffusion time scale is not true at low currents. To be sure that a negative (positive) H implies that few (many) runaways will be produced, $|H|$ should be at least about 5. In simulations where the background density is taken to increase during the thermal quench it is n_{e} at the time of maximum primary generation that determines the efficiency of primary current conversion, not the initial density. The simulations for different T_{final} in Fig. 5 are especially interesting because T_{final} is not known from measurements, but it has been conjectured to be around 10 eV.[4] This conjecture is supported by the simulations, since Figs. 5 and 2(b) show that the simulation with $T_{\text{final}}\sim 10$ eV reproduces the experimental measurements of the reference JET discharge in terms of current conversion ratio and time scale of the current drop.

The simulations in Fig. 6 with different plasma cooling time scales show that for realistic t_0 values ($\lesssim 0.5$ ms) the final current and runaway density profiles are insensitive to t_0. This is because the time scale of primary production, which is determined by t_0, is much smaller than the avalanche and electric-field diffusion time scales. Even though the onset of primary production changes with different t_0 values, this does not affect the later stages, because the seed profile is very similar. This also shows that for realistic t_0 the approximation used in the derivation of the H criterion, that the thermal quench is infinitely fast, is acceptable. For unrealistically long cooling times ($t_0\gtrsim 5$ ms) the time scales are no longer separated and the avalanche is relatively more important since it commences already during the main stage of primary generation. Since runaway production is now a slower process, there is time to lose a larger part of the electric field by resistive diffusion, which results in a lower total final current [see Fig. 6(b)].

Another interesting parameter to consider is the time of onset of the thermal quench. It is likely that the thermal quench starts at different times in different parts of the plasma. In order to model a cold front propagating from the edge inwards, we take

$$T_e - T_{e,\text{final}} \propto \frac{1}{2}\left[1-\tanh\frac{(t-t_{\text{quench}}(r))/t_0}{2}\right], \tag{20}$$

with

$$t_{\text{quench}}(r)=\bar{t}_{\text{quench}}(1-r/a). \tag{21}$$

The simulations in Fig. 7 show that if the delay $\bar{t}_{\text{quench}}$ between the edge and the center of the plasma is comparable to the diffusion time scale the final current profile becomes

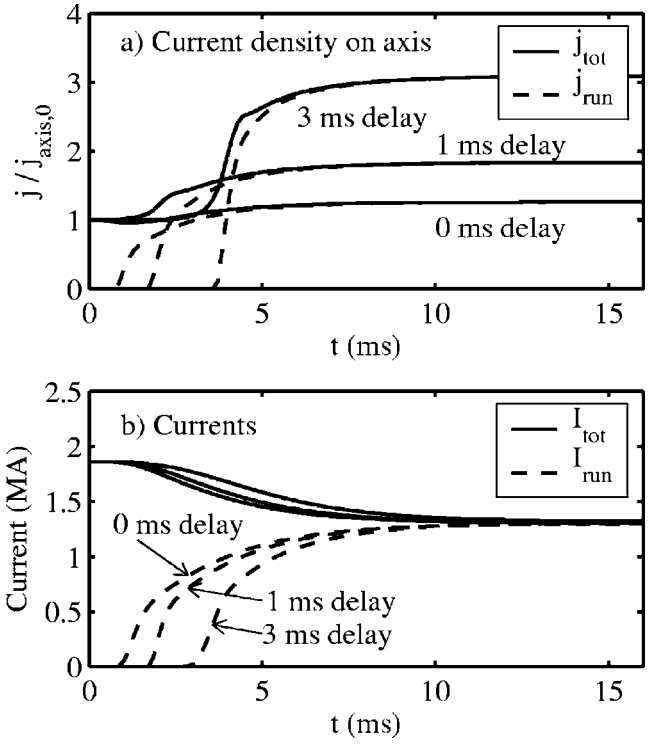

FIG. 7. Simulations where the thermal quench starts at different times depending on radius according to Eq. (21). The delay between the boundary and the center of the plasma is $\bar{t}_{\text{quench}}=0$, 1, and 3 ms.

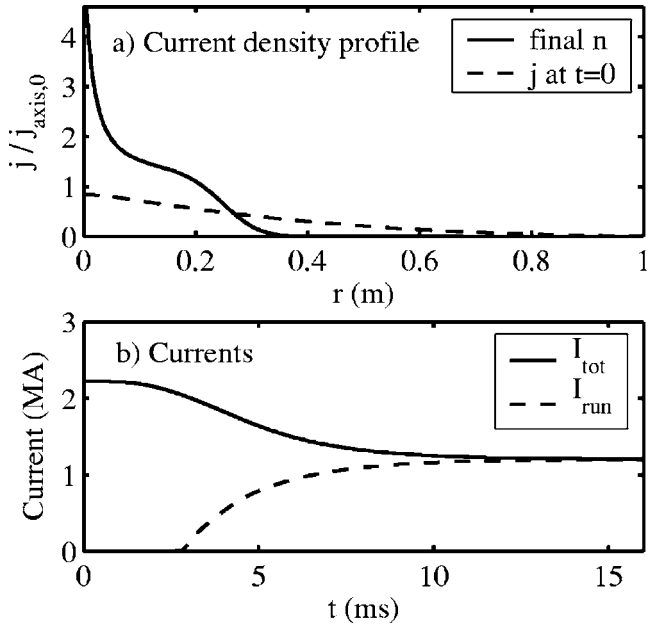

FIG. 8. An example of a more complex disruption scenario that can arise due to gas puffs or pellet injection. Here n_e rises to $3n_{e0}$ and Z_{eff} increases from 1 to 1.5 during the thermal quench, and the onset is delayed 2 ms from the plasma boundary to the magnetic axis.

more peaked than it would have without the delay. This effect is due to the fact that the electric field first rises at the edge and has time to diffuse inwards before the cold front has reached the center. This also has the effect that the on-axis Ohmic current density rises slightly before the local thermal quench time. Even though the current profile becomes more peaked on axis with increasing $\bar{t}_{\text{quench}}$ the final total current in Fig. 7(b) appears to be unaffected.

When particles with $Z>1$ enter the plasma during the disruption, either as impurities from the wall or due to intentional impurity gas puffing or pellet injection, the conductivity $\sigma_{\parallel}$ falls since it is approximately proportional to Z_{eff}^{-1}. This drop in conductivity has a larger effect on primary generation than that due to cooling, because $E_{\text{D}} \propto T_e$ while E_{D} is independent of Z_{eff}. The primary and secondary runaway generation rates, Eqs. (1) and (3), are also modified for $Z_{\text{eff}} \neq 1$, but the dominant effect is from the increased electric field due to the drop in conductivity. A simulation where Z_{eff} increases on the time scale of the thermal quench from 1 to 5 shows an enhanced primary runaway production and it yields a current conversion ratio of 84%, which should be compared with 69% for the reference case where the ion charge is taken to be constant $Z_{\text{eff}}=1$.

More complex disruption scenarios can also be simulated, and especially important are simulations that try to predict the efficiency of different runaway electron mitigation schemes.[21] The aim of these techniques is to produce a controlled disruption with reduced runaway generation. This can be done by injecting low-Z material into the discharge and thereby increasing the background electron density so that both E_{D} and E_c rise. This kind of disruption is more complex than the scenarios we have discussed so far. Both the background density and effective charge change during the thermal quench, and the time of onset of the thermal quench depends on plasma radius. Figure 8 presents a simulation of such a scenario, where n_e rises to $3n_{e0}$ and Z_{eff} increases from 1 to 1.5 during the thermal quench, and the onset is delayed 2 ms from the plasma boundary to the magnetic axis. The result is a dramatic, and probably undesirable, peaking of the current profile near the magnetic axis, which would result in MHD instability.

It is also interesting to consider what happens if some plasma parameter has a small-scale radial variation due to the properties of the predisruption plasma or the instability leading up to the disruption. An example is given in Fig. 9, where the final current profile is shown for a simulated disruption with a 4% ripple in the thermal quench time, $t_0=0.5\ \text{ms}\times[1+0.02\sin(40\pi x)]$. Despite the smallness of this variation, the runaway current becomes almost completely filamented. The physical reason for this is that the

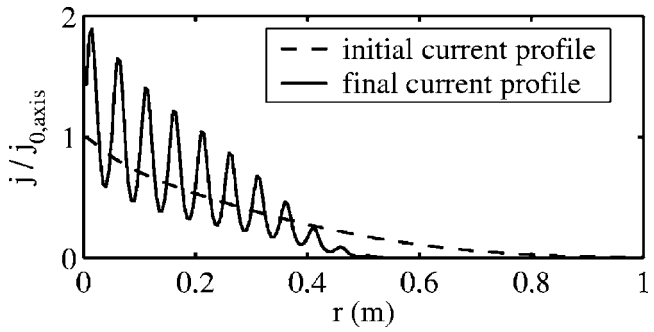

FIG. 9. The final current profile from a simulation where t_0 has a 4% radial ripple.

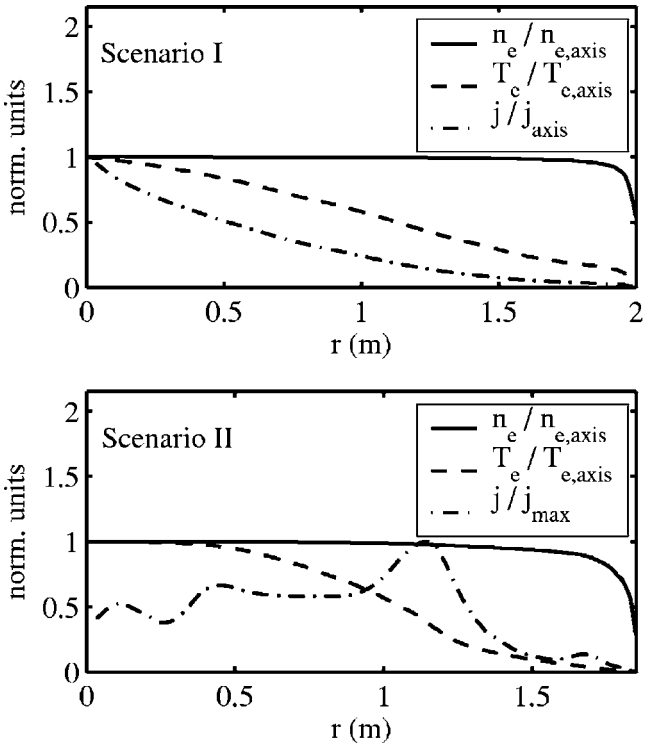

FIG. 10. Predisruption density, temperature, and current profiles for two different ITER scenarios.

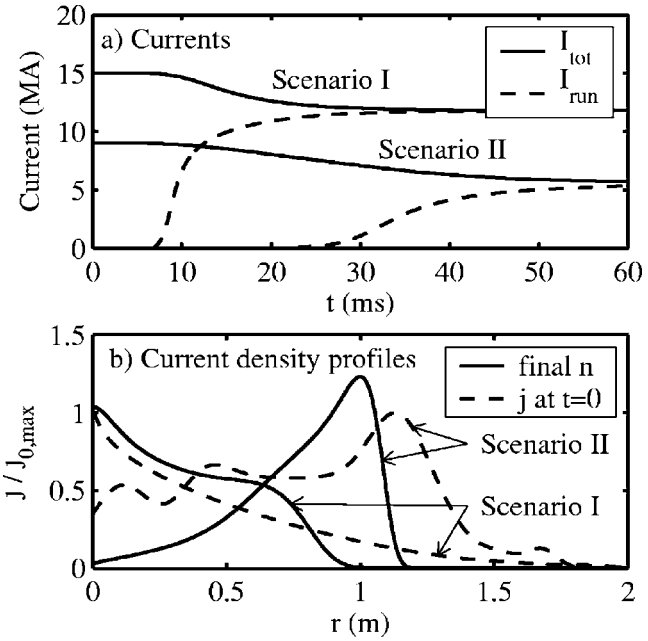

FIG. 11. Simulations of the runaway dynamics in ITER disruptions for scenarios I and II in Fig. 10.

primary runaway production rate is extremely sensitive to plasma parameters, and will be investigated in more detail in the next section. In view of this result, it appears likely that the postdisruption runaway current will never be entirely smooth. It is tempting to speculate that this may explain why hard x rays emitted when the runaway plasma hits the vessel wall usually appear in a series of sharp bursts.[19]

B. ITER

The agreement between theory and experiment that we have found in the case of JET gives confidence that our model can be used for ITER predictions, at least unless other runaway production mechanisms are important. Runaway "bursting" associated with the finite duration of the thermal quench might be particularly effective in ITER (Ref. 14), but for the purposes of the present paper we adhere to the model used so far.

ITER disruption simulations using the two different density, initial temperature, and initial current profiles in Fig. 10 have been performed and the results are shown in Fig. 11. The parameters for scenario I are: $R=6.2$ m, $a=2.0$ m, $I_0=15$ MA, $\bar{n}_e=10.6\cdot10^{19}$ m^{-3}, $\bar{T}_{e0}=22.7$ keV, and for scenario II: $R=6.35$ m, $a=1.85$ m, $I_0=9$ MA, $\bar{n}_e=7.1\cdot10^{19}$ m^{-3}, $\bar{T}_{e0}=30$ keV. Scenario I is an ITER plasma with inductive current[1] and scenario II is a steady-state case with noninductive current.[22] In these simulations a flat temperature profile of 10 eV is assumed after the thermal quench, the thermal quench time is $t_0=1$ ms, and $q=2.5$ is used for calculating the neoclassical correction to the conductivity in Eq. (9). To be able to treat the noninductive current in scenario II using our model, the initial electric field is artificially set to $E_{\|0}=j_{\|0}/\sigma_{\|0}$. This is not the correct predisruption electric field, but it gives the right initial current profile and the right induced field after the thermal quench, so the simulations indeed produce the correct postdisruption current dynamics. Secondary generation is more important in scenario II compared with scenario I, partly because of the lower initial current, and consequently the current falls on a longer time scale as seen in Fig. 11(a). The final runaway current profile [Fig. 11(b)] becomes peaked *off axis* in the noninductive scenario, because of the shape of the initial current profile.

Some general differences between JET and ITER can be seen if one compares Fig. 2 with scenario I in Fig. 11. The density and the initial temperature are higher in ITER, so it takes a longer time to reach sufficiently low temperature to initiate the primary generation. Due to the higher current, secondary generation is more effective in ITER than in JET relative to primary generation. The current conversion ratio is also higher in ITER than in JET, and would become even higher if additional runaway production mechanisms were included.

The same trends that are seen when varying parameters around a JET discharge are also seen when an ITER discharge is studied. Low current ($I_0\lesssim4$ MA) or high electron density ($n_{e0}\gtrsim1\cdot10^{21}$ m^{-3}) simulations show no runaways. Moderate currents ($I_0\sim4-30$ MA) or moderate densities ($n_{e0}\sim10^{19}-10^{21}$ m^{-3}) give peaked profiles, while even higher currents or lower densities cause primary generation to be enormous and to effectively reproduce the initial current profile in the postdisruption plasma.

IV. ANALYTICAL TREATMENT

Many of the features of the numerical simulations described in the previous section can be understood analyti-

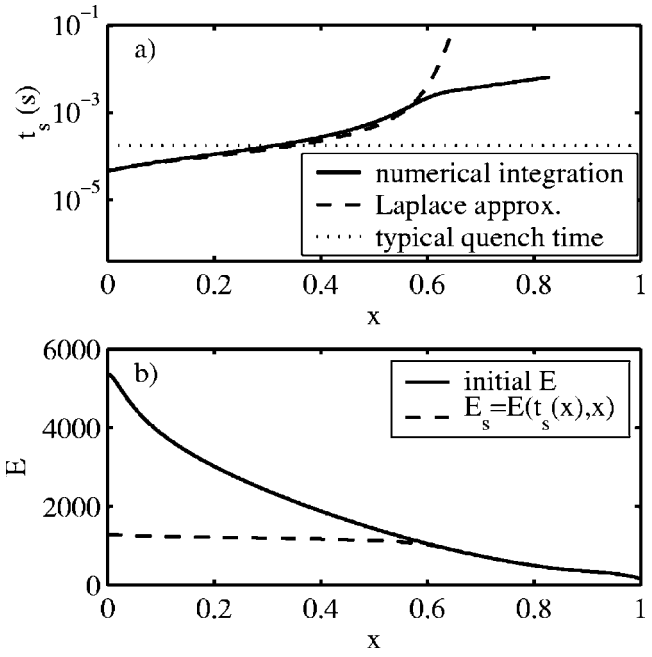

FIG. 12. (a) The time $t_s(x)$ at which secondary generation overtakes primary generation as numerically calculated from the integral in Eq. (27) and also from the analytical approximation of the integral using Laplace's method. A typical disruption time t_0=0.5 ms is shown for reference. (b) The electric field $E_s=E(t_s(x),x)$.

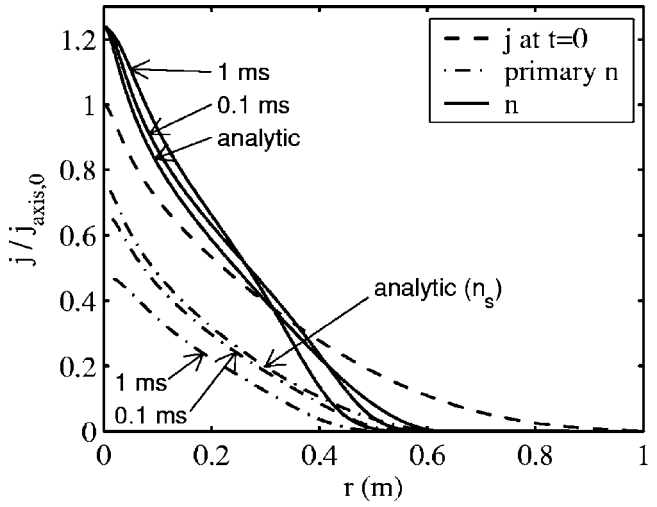

FIG. 13. Analytical current profiles and profiles for simulations with different t_0. The analytic runaway seed approximation n_s in Eq. (26) is approached by the simulated profiles of accumulated primary production for fast thermal quenches, and the simulated total runaway production approaches the solution to Eq. (32). Compare with Fig. 6(a).

cally by noting that there is usually a separation of time scales between primary generation and electric-field diffusion. We thus divide the problem into two stages. In the first stage, the runaway "seed" is generated by primary production and may be amplified somewhat by secondary generation, but there is no radial diffusion of electric field. In the second and much longer stage, runaway avalanching and radial diffusion of the electric field operate in parallel, but primary production can be neglected.

A. First stage: Establishing a runaway seed profile

The radial profile of the runaway seed $n_\star(x)$ can be calculated under the following simplifying assumptions:

(1) Diffusion is negligible on the short time scale of primary generation.
(2) The thermal quench is taken to be infinitely fast.

The first assumption implies that the current density $n+\sigma E=j_0(x)$ (where $j\equiv j_\parallel/\bar{j}_{\parallel 0}$) is independent of time. The second assumption makes the conductivity jump from σ_{0-} to σ_{0+} at $t'=0$, so that the electric field just after the thermal quench becomes

$$E(x)=E_{0+}(x)=\frac{j_0(x)}{\sigma_{0+}(x)}. \tag{22}$$

In practice, this electric field is very large, $E\gg 1\geq n_e/\bar{n}_{e0}$ and the first model equation (16) becomes $\partial n/\partial t'-nE=F(E)$, or equivalently

$$-\sigma_{0+}\frac{\partial E}{\partial t'}-(j_0-\sigma_{0+}E)E=F(E). \tag{23}$$

This equation can be solved independently for each radius x (since diffusion has been neglected), giving $E(t')$ implicitly as

$$\begin{aligned} t' &= \int_E^{E_{0+}} \frac{dE'}{F(E')/\sigma_{0+}+E_{0+}E'-E'^2} \\ &\simeq \int_{E_s}^{E_{0+}} \frac{\sigma_{0+}dE'}{F(E')}+\int_E^{E_s}\frac{dE'}{E_{0+}E'-E'^2} \\ &= t_s+\frac{1}{E_{0+}}\ln\frac{(E_{0+}-E)E_s}{(E_{0+}-E_s)E}. \end{aligned} \tag{24}$$

Recognizing that primary production depends extremely sensitively upon E, see (18), and therefore "switches off" very quickly when E drops, we have approximated the integral (24) as a sum of two terms, where primary runaway production dominates in the first one (when $E>E_s$) and is absent in the second one (when $E<E_s$). The time $t_s(x)$ at which $E=E_s$ and secondary generation overtakes primary generation at the location x is given by

$$F(E_s)=(j_0-\sigma_{0+}E_s)E_s=n_sE_s, \tag{25}$$

where $E_s(x)=E(x,t_s(x))$. A numerical solution of Eq. (25) is presented in Fig. 12, where it is seen that $t_s(x)$ is very small in the center of the plasma where most runaways are eventually generated. Primary runaway generation is thus only important in an initial transient, as we already noted in the previous section. Equation (25) provides a good approximation for the number of primary runaways,

$$n_s(x)=\frac{F(E_s)}{E_s}=j_0E_s\left(1-\frac{E_s}{E_{0+}}\right). \tag{26}$$

Figure 13 shows that in full simulations of Eqs. (16) and (17)

the profile of the accumulated primary runaway density during the disruption indeed approaches the approximation (26) as the thermal quench time becomes small.

The time $t_s(x)$ can be determined in the following way: Define $-f(E)$ as the exponent and $g(E)$ as the preexponential factor in the expression for primary generation (18), so that $F(E)=g(E)e^{-f(E)}$. If E_s is known from the solution of Eq. (25), then $t_s(x)$ can be calculated from the integral

$$t_s(x)=\sigma_{0+}\int_{E_s}^{E_{0+}}\frac{e^{f(E')}dE'}{g(E')}\simeq\frac{\sigma_{0+}e^{f(E_s)}}{g(E_s)|f'(E_s)|}=\frac{\sigma_{0+}}{n_sE_s|f'(E_s)|}. \tag{27}$$

Laplace's method[23] is used in the above approximation of the integral. This approximation is only valid for small x, because E_s is very near E_{0+} at large x, where primary generation takes a long time to build up. As a typical case, t_s for the JET reference discharge used above is shown in Fig. 12.

Solving Eq. (24) for E and using $n=j_0-\sigma_{0+}E$ we obtain the runaway profile at a time $t'>t_s$,

$$n(t',x)=j_0\left[1-\left(e^{E_{0+}(t'-t_s)}\frac{E_{0+}-E_s}{E_s}+1\right)^{-1}\right]. \tag{28}$$

In a real disruption with nonzero t_0, this expression can be expected to be accurate if $t_0<\min t_s(x)$ ($t_0\lesssim 0.1$ ms in the reference case). Simulations of the full model equations show that the time of equal primary and secondary generation has a maximum and then decreases as x approaches 1 because of field diffusion at the plasma edge. Thus Eq. (28) is only a good approximation for small x, and it is therefore permissible to use the Laplace approximation (27) for t_s. In conclusion, Eq. (28) gives an approximation of the seed profile $n_\star=n(t_\star,x)$ for small x if $t_\star$ is chosen as a sufficiently late time where field diffusion has not yet become important.

B. Second stage: Runaway avalanche

For $t'>t_\star$ the electric field has become small enough that primary runaway production is negligible, and the plasma current evolves due to runaway avalanching and diffusion of the electric field. When primary production is neglected in Eqs. (16) and (17), these equations can be combined into the single equation

$$\nabla^2\frac{\partial N}{\partial t'}=\alpha\frac{\partial}{\partial t'}\left(\sigma\frac{\partial N}{\partial t'}+e^N\right), \tag{29}$$

where $N\equiv\ln n$ and

$$\nabla^2=\frac{1}{x}\frac{\partial}{\partial x}x\frac{\partial}{\partial x}. \tag{30}$$

Equation (29) can be integrated once with respect to time to yield

$$\sigma\frac{\partial N}{\partial t'}=\frac{1}{\alpha}\nabla^2(N-N_\star)+j_\star-e^N. \tag{31}$$

This equation links the seed profile $N_\star(x)=N(t_\star,x)$ and the total current profile $j_\star$ at $t'=t_\star$ to the runaway current profile at later times. In particular, an equation for the final current profile is obtained by setting $\partial N/\partial t'=0$, giving

$$\frac{1}{\alpha}\nabla^2(N-N_\star)+j_\star-e^N=0. \tag{32}$$

If the electric-field diffusion is negligible at times $t'<t_\star$, then $j_\star$ is approximately equal to the initial current profile. Therefore, if $N_\star(x)$ has been calculated as in the previous subsection, then the problem of determining the final current profile has been reduced to the ordinary differential equation [(32)] with the boundary conditions $\partial N/\partial x=0$ at $x=0$ and $N=N_\star$ at $x=1$ (no runaway generation at the boundary, where the electric field is small). Before we proceed to solve Eq. (32) numerically, a number of important analytical results can immediately be derived from it.

One exact mathematical result is that the final current is always smaller than the predisruption current, as always observed in experiment. This follows by taking the first moment of Eq. (32)

$$\int_0^1(j_\star-e^N)xdx=-\frac{1}{\alpha}\left.\frac{d(N-N_\star)}{dx}\right|_{x=1}\geq 0, \tag{33}$$

since there are no runaways on the boundary and $N(x)\geq N_\star(x)$ for all x.

Another exact result is that $N(x)$ is always peaked on axis if

$$G(x)\equiv j_\star(x)-\alpha^{-1}\nabla^2N_\star(x) \tag{34}$$

is a monotonically decreasing function; or more generally, if

$$\int_0^x G(x')x'dx'<G(0)\int_0^x x'dx' \tag{35}$$

for all x. To see that this implies $\nabla^2N(0)=2N''(0)<0$, assume the opposite: $N''(0)>0$. Then $N'(x)>0$ in some interval $0<x<x_1$, where x_1 is the first zero of $N'(x)$. It follows that $N(x)>N(0)$ on this interval and hence

$$\int_0^{x_1}(e^N-G(x))xdx>\int_0^{x_1}(e^{N(0)}-G(0))xdx$$
$$=\int_0^{x_1}\alpha^{-1}\nabla^2N(0)xdx>0, \tag{36}$$

but according to Eq. (32), this integral is equal to

$$\int_0^{x_1}\alpha^{-1}\nabla^2N(x)xdx=\alpha^{-1}x_1N'(x_1)=0, \tag{37}$$

which is a contradiction. That the runaway current is peaked on axis comes as no surprise, of course, and is consistent with all the simulations in the previous section. These simulations also showed that the runaway current density on axis often exceeds the predisruption current density there, i.e., $e^{N(0)}>1$. This increment in central current density cannot be arbitrarily large, however. From $\nabla^2N(0)<0$ and Eq. (32), we immediately find an upper bound on the central runaway current density,

$$e^{N(0)} \leq j_\star(0) - \frac{1}{\alpha}\nabla^2 N_\star(0). \tag{38}$$

In practice, the current density is usually far from this upper bound.

Another interesting property of Eq. (32) is that it predicts that the runaway current can easily acquire large radial variations locally, as we saw in Fig. 9. This is perhaps surprising since the electric field satisfies a diffusion equation, which by nature smoothens its profile. However, since the highest derivative in Eq. (32) operates on the difference $N-N_*$, it implies that if $N_\star$ makes a sudden jump at some radial location, then a similar discontinuity is reflected in N,

$$N(x+) - N(x-) = N_\star(x+) - N_\star(x-). \tag{39}$$

If most runaways are generated by the secondary mechanism, $e^N \gg e^{N_\star}$, then this implies that fine-scale structure in the seed profile $n_\star = e^{N_\star}$ is *amplified* by the secondary avalanche. If the seed profile varies from, say, 1 $\mathrm{kA/m^2}$ to 2 $\mathrm{kA/m^2}$ in a sufficiently short radial distance, then the final current density profile will vary from perhaps 1 $\mathrm{MA/m^2}$ to 2 $\mathrm{MA/m^2}$. The *relative* jump is the same by Eq. (39) but the *absolute* one is much larger. For small variations, this can be seen more quantitatively by linearizing Eq. (32) around some known solution $N=N_0(x)$ corresponding to a seed profile $N_{\star 0}(x)$. Taking the perturbed seed profile to be $N_\star(x)=N_{0\star}(x)(1+\varepsilon \sin kx)$, where $\varepsilon \ll 1 \ll k$, and writing $N(x)=N_0(x)+N_1(x)$ with $N_1(x) \ll 1$, we obtain the perturbed solution as

$$N_1(x) \simeq \frac{\varepsilon k^2 N_{0\star} \sin kx}{\alpha e^{N_0(x)} + k^2}, \tag{40}$$

which indicates that the relative variation in $N_\star$ is mirrored in $N_1(x) \simeq \varepsilon \sin kx$ for sufficiently small-scale $(k^2 \gg \alpha)$ variations.

Direct numerical solution of Eq. (32) can easily be performed. Since $j_\star = j_0$ dominates over e^N for large x, the quantity $N-N_\star$ in Eq. (32) is independent of the seed profile for large x. One is therefore allowed to take $N_\star$ from the seed profile calculated in Eq. (28), which holds for small x. In most cases it is even a good approximation to use $N_\star \simeq \ln n_s$ from Eq. (26), which also removes the ambiguity introduced by the choice of $t_\star$. The final current profile obtained in this way for the reference JET discharge is shown in Fig. 13, and it is seen that the current profiles from full simulations of the model equations approach the solution to Eq. (32) for sufficiently fast disruptions.

V. CONCLUSIONS

In this paper, we have developed and explored a relatively simple model for the evolution of the current, including that carried by runaway electrons, in a tokamak disruption. The model consists of an equation for the generation of runaway electrons coupled to a diffusion equation for the electric field. As the plasma cools down in the thermal quench of the disruption and a large toroidal field is induced which accelerates runaways, the current carried by these short circuits the plasma and reduces the electric field, which, however, continues to generate new runaways until it has diffused out of the plasma. If no diffusion occurred, the final plasma current (which is entirely carried by runaways) would be almost the same as the predisruption current, and their radial profiles would also be the same. It is the diffusion of electric field that enables the plasma current to change and thus controls what fraction of the predisruption current is converted to runaway electrons. In JET this fraction is observed to be up to 50%–60%, which agrees well with our simulations if we choose the postdisruption electron temperature to be around 10 eV. This is in accordance with other estimates of the postdisruption temperature, and also makes the time scale and the measured toroidal electric field agree (roughly) with the measurements.

The model equations are nonlinear and describe a range of different possible evolution scenarios for the disrupting plasma. To illustrate these, we have performed numerical simulations in a parameter scan around a typical JET disruption discharge. Three qualitatively different regions of parameter space can be discerned: one with very few runaways, a second with high on-axis current peaking and predominantly secondary runaway generation, and a third where primary generation alone reproduces the initial current profile. An analytical solution of a reduced, zero-dimensional version of the model equations indicates that the limit between the first and second regions can roughly be expressed as a simple criterion in terms of the parameter H defined in Eq. (A10). A substantial amount of runaway current is only produced if H is positive.

Some analytical insight is also possible into the unreduced, one-dimensional system. Because of the rapidity of primary runaway generation, the evolution of the current can be divided into two stages. The first stage is short enough that resistive diffusion can be neglected, and produces a seed of runaways which is amplified in the second stage, where primary generation is instead neglected. This enables the derivation of equations that can be used for semianalytical calculations of the final current profile in sufficiently fast disruptions. Furthermore, two more qualitative conclusions can be drawn from the analysis.

First, because the runaways are most easily generated in the center of the plasma where the relative change in conductivity is largest, this is where they will first short circuit the torus and limit the growth of the electric field. Some short time after the thermal quench, the radial profile of the toroidal electric field will therefore be hollow and have an off-axis maximum. This enables the field to diffuse radially inward, leading to even more runaways being created in the center of the plasma and causing the postdisruption current profile to become more peaked than the predisruption current. Although the total current falls in the disruption, it is possible that the current density rises in the center. Interestingly, this is not only observed in numerical solutions of the model equations, but may already have been observed on JET. Reference 24 reports a measurement of the runaway current profile after a disruption indicating a very low safety factor on axis, $q \simeq 0.6$, suggesting that the central current density may have increased as a result of the disruption. The

implications of this phenomenon for resistive plasma stability are under investigation.

A second prediction of the theory is that the runaway electron current may very easily become radially filamented. Because the toroidal electric field is much smaller than the Dreicer field, the rate of primary runaway generation is exponentially sensitive to plasma parameters. For instance, if the density on one flux surface is slightly lower than on the neighboring ones, far more primary runaways are generated there and, importantly, this difference is amplified by the secondary avalanche. This may explain why the x-ray signal emitted when runaways hit the vessel wall is usually very bursty.

Disruption-generated runaway electrons are widely believed to pose a potentially serious problem for ITER, and the theory presented in this paper corroborates this view. The fraction of the predisruption current that is converted to runaways is predicted to be higher than in present experiments, and the current profile could evolve far from its initial shape, making postdisruption stability control difficult. It is thus desirable to develop runaway mitigation techniques, e.g., based on the injection of gas, pellets, or liquid jets. The theory developed in this paper lends itself to modeling such schemes, which is a topic we intend to pursue in the near future.

ACKNOWLEDGMENTS

This work was funded by EURATOM under association contracts with the United Kingdom, Sweden, and France, and by the UK Engineering and Physical Sciences Research Council. The views and opinions expressed herein do not necessarily reflect those of the European Commission.

APPENDIX: A SIMPLE CRITERION FOR SUBSTANTIAL RUNAWAY PRODUCTION

A zero-dimensional model of the current dynamics using only on-axis quantities (denoted by an overhead bar) gives two coupled *ordinary* differential equations.[5] By introducing a characteristic radial length scale Δ, and approximating $\nabla^2 E_\parallel \simeq -\bar{E}_\parallel/\Delta^2$ and $I \simeq \bar{j}_\parallel 2\pi\Delta^2$, we can replace the induction equation (6) by

$$\bar{E}_\parallel = -\frac{L}{2\pi R}\frac{dI}{dt}, \tag{A1}$$

where the major radius of the torus is R and the plasma inductance is $L=R\mu_0$. The zero-dimensional model is thus governed by the equations

$$\frac{d\bar{n}}{dt'} = [F(\bar{E}) + \bar{n}(\bar{E}-1)]\Theta(\bar{E}-1), \tag{A2}$$

$$-\frac{\bar{E}}{\tilde{\alpha}} = \frac{d}{dt'}(\bar{\sigma}\bar{E} + \bar{n}), \tag{A3}$$

where the thermal electron density is assumed to be constant in time, $\bar{n}_e = \bar{n}_{e0}$, and

$$\tilde{\alpha} = \frac{\sqrt{2\pi}}{3}\frac{I_0}{I_A \ln\Lambda}. \tag{A4}$$

Equations (A2) and (A3) cannot be solved analytically, but it is possible to derive from them a criterion for whether or not substantial runaway production will occur. Thus, from knowing only basic plasma parameters (density, temperature, current, etc.) it is possible to predict whether or not a major fraction of the predisruption current is converted to runaway electrons.

As can be seen in Sec. III, most runaways are not generated during the thermal quench itself but are instead produced during the decay of the electric field, which occurs on the resistive time scale L/R. The thermal quench can thus be taken to occur infinitely fast, at the time $t'=0$, say. No runaways are then generated initially and the current does not change from $t'=0^-$ to $t'=0^+$. The conductivity drops form its predisruption value $\bar{\sigma}_{0-}$ to $\bar{\sigma}_{0+}=(\bar{T}_{0+}/\bar{T}_{0-})^{3/2}\bar{\sigma}_{0-}$, and since the current is constant, $\bar{\sigma}\bar{E}=1$, the electric field rises from $\bar{E}_{0-} \ll 1$ to some large value $\bar{E}_{0+}=1/\bar{\sigma}_{0+} \gg 1$. We assume that the temperature is constant after the thermal quench, so that $\bar{\sigma}(t')=\bar{\sigma}_{0+}$ for all $t'>0$ and consider the ratio of Eqs. (A3) and (A2),

$$\bar{\sigma}_{0+}\frac{d\bar{E}}{d\bar{n}} = -1 - \frac{\bar{E}}{\tilde{\alpha}[F(\bar{E}) + \bar{n}\bar{E}]}. \tag{A5}$$

Initially there are no runaway electrons, so Dreicer generation will dominate and

$$\bar{\sigma}_{0+}\frac{d\bar{E}}{d\bar{n}} = -1 - \frac{\bar{E}}{\tilde{\alpha}F(\bar{E})}. \tag{A6}$$

There are two interesting limits of this equation. If the first term on the right dominates, primary generation is so efficient that the runaway current completely replaces the initial Ohmic current. The other limit is when the second term dominates, and the primary mechanism only generates a small runaway population, $\bar{n}_\star \ll 1$, which is given by

$$\bar{n}_\star = \tilde{\alpha}\bar{\sigma}_{0+}\int_{\bar{E}_\star}^{\bar{E}_{0+}} \frac{F(\bar{E})d\bar{E}}{\bar{E}} \simeq 4\tilde{\alpha}\bar{\sigma}_{0+}u^2\bar{E}_{0+}F(\bar{E}_{0+}). \tag{A7}$$

It is now possible to estimate the combined effect of primary and secondary generation, by noting that the time scale of primary production is much shorter than the avalanche time scale. The role of primary production is mainly to provide a small "seed" for the secondary avalanche. After some short time, $t_\star$, when the runaway density is $\bar{n}_\star$, most subsequent runaways will be produced by the secondary mechanism, and Eq. (A5) can be simplified to

$$\frac{d\bar{n}}{d\bar{E}} = -\frac{\bar{\sigma}_{0+}\tilde{\alpha}\bar{n}}{1+\tilde{\alpha}\bar{n}} \tag{A8}$$

in the limit $\bar{E} \gg 1$. The effect of the $\tilde{\alpha}\bar{n}$ term in the denominator is to limit $\bar{n}$, so that the runaway current eventually cannot exceed the initial current. Initially, when $\bar{n} \ll \tilde{\alpha}^{-1}$, this term is small and we neglect it to see whether at all the

runaway density can reach higher values. The equation then describes the purely exponential avalanche effect, which increases the runaway population by a factor $e^{\tilde{\alpha}}$, since for $\bar{E} \ll \bar{E}_\star \simeq \bar{E}_{0+}$ the number of runaways becomes $\bar{n}=\bar{n}_\star e^{\tilde{\alpha}\bar{\sigma}_{0+}\bar{E}_{0+}}=\bar{n}_\star e^{\tilde{\alpha}}$. Hence, the combined primary and secondary production is

$$\begin{aligned}\bar{n} &= 4\tilde{\alpha}\bar{\sigma}_{0+}u^2\bar{E}_{0+}F(\bar{E}_{0+})e^{\tilde{\alpha}} \\ &= \frac{\sqrt{2}}{\pi}\tilde{\alpha}\ln\Lambda\left(\frac{\bar{E}_{\mathrm{D}0+}}{\bar{E}_{\|0+}}\right)^{11/8}u^{-2} \\ &\quad\times\exp\left(\tilde{\alpha}-\frac{\bar{E}_{\mathrm{D}0+}}{4\bar{E}_{\|0+}}-\sqrt{\frac{2\bar{E}_{\mathrm{D}0+}}{\bar{E}_{\|0+}}}\right).\end{aligned} \tag{A9}$$

If pre-exponential factors other than powers of u and $E_\|/E_\mathrm{D}$ are neglected, the logarithm of this expression is approximately

$$H \equiv \tilde{\alpha}-\frac{\bar{E}_{\mathrm{D}0+}}{4\bar{E}_{\|0+}}-\sqrt{\frac{2\bar{E}_{\mathrm{D}0+}}{\bar{E}_{\|0+}}}+\ln\frac{m_e c^2}{\bar{T}_{e0+}}+\frac{11}{8}\ln\frac{\bar{E}_{\mathrm{D}0+}}{\bar{E}_{\|0+}}, \tag{A10}$$

which corrects and refines a similar result in Ref. 5. The dimensionless number H encapsulates the strength of primary (last four terms) and secondary (first term) runaway production in an approximate way. It is not a reliable estimate for the actual number of runaways produced in a disruption, since the term responsible for saturation in Eq. (A8) was neglected, but it does indicate whether or not substantial runaway production will occur. If H is negative, only a small fraction of the predisruption current is converted into runaways, while $H>0$ indicates that a large runaway current can appear. From a practical point of view, it is useful to note that Eq. (A10) can be expressed in terms of simple plasma parameters by relating $\bar{E}_{0+}=1/\bar{\sigma}_{0+}$ to the safety factor q by $j_\|=\sigma_\mathrm{Sp}E_\|=2B/\mu_0 qR$, which gives

$$\frac{\bar{E}_{\|0+}}{\bar{E}_{\mathrm{D}0+}}=\frac{3\mu_0 e n_e q R}{B}\sqrt{\frac{\pi\bar{T}_{e0+}}{2m_e}}. \tag{A11}$$

[1] R. Aymar, P. Barabaschi, and Y. Shimomura (for the ITER team), Plasma Phys. Controlled Fusion **44**, 519 (2002).
[2] P. H. Rebut, R. J. Bickerton, and B. E. Keen, Nucl. Fusion **25**, 1011 (1985).
[3] H. Ninomiya and the JT-60U Team, Phys. Fluids B **4**, 2070 (1992).
[4] J. A. Wesson, R. D. Gill, H. Hugon *et al.*, Nucl. Fusion **29**, 641 (1989).
[5] P. Helander, L.-G. Eriksson, and F. Andersson, Plasma Phys. Controlled Fusion **44**, B247 (2002).
[6] L.-G. Eriksson, P. Helander, F. Andersson, D. Anderson, and M. Lisak, Phys. Rev. Lett. **92**, 205004 (2004).
[7] P. Helander, F. Andersson, L.-G. Eriksson, T. Fülöp, H. Smith, D. Anderson, and M. Lisak, *Proceedings of the 20th International Conference on Fusion Energy, Vilamoura, 2004* (IAEA, Vienna, 2005), TH/P4-39.
[8] J. W. Connor and R. J. Hastie, Nucl. Fusion **15**, 415 (1975).
[9] A. V. Gurevich, Sov. Phys. JETP **12**, 904 (1961).
[10] R. H. Cohen, Phys. Fluids **19**, 239 (1976).
[11] P. Helander and D. J. Sigmar, *Collisional Transport in Magnetized Plasmas* (Cambridge University Press, Cambridge, 2002), p 43.
[12] M. N. Rosenbluth and S. V. Putvinski, Nucl. Fusion **37**, 1355 (1997).
[13] M. N. Rosenbluth, P. B. Parks, D. Post, S. Putvinski, N. Putvinskaya, H. A. Scott, and the ITER Joint Central Team, *Proceedings of the 16th International Conference on Fusion Energy, Montreal, 1996* (IAEA, Vienna, 1997), IAEA-CN-64/FP-26.
[14] H. Smith, P. Helander, and T. Fülöp, Phys. Plasmas **12**, 122505 (2005).
[15] J. Wesson, *Tokamaks* (Clarendon, Oxford, 2004), p. 735.
[16] R. Jaspers, N. J. Lopes Cardozo, F. C. Schüller, K. H. Finken, T. Grewe, and G. Mank, Nucl. Fusion **36**, 367 (1996).
[17] J. R. Martín-Solís and R. Sánchez, Phys. Plasmas **7**, 3369 (2000).
[18] V. V. Plyusnin, V. Riccardo, R. Jaspers, B. Alper, V. G. Kiptily, J. Mlynar *et al.*, Nucl. Fusion **46**, 277 (2006).
[19] R. D. Gill, Nucl. Fusion **33**, 1613 (1993).
[20] L.-G. Eriksson and P. Helander, Comput. Phys. Commun. **154**, 175 (2003).
[21] S. Putvinski, P. Barabaschi, N. Fujisawa, N. Putvinskaya, M. N. Rosenbluth, and J. Wesley, Plasma Phys. Controlled Fusion **39**, B157 (1997).
[22] ITER Technical Basis, Plant Description Document, ITER Engineering Design Activities Documentation Series No. 24 (IAEA, Vienna, 2002), Chap. 4, p. 12.
[23] C. M. Bender and S. A. Orszag, *Advanced Mathematical Methods for Scientists and Engineers* (Springer-Verlag, New York, 1999).
[24] R. D. Gill, B. Alper, A. W. Edwards, L. C. Ingesson, M. F. Johnson, and D. J. Ward, Nucl. Fusion **40**, 163 (2000).